PNAS RESEARCH ARTICLE | ENVIRONMENTAL SCIENCES
EARTH, ATMOSPHERIC, AND PLANETARY SCIENCES OPEN ACCESS

Impact of warming on aquatic body sizes explained by metabolic scaling from microbes to macrofauna

Curtis Deutsch[a,b,c,1], Justin L. Penn[a,b], Wilco C. E. P. Verberk[d], Keisuke Inomura[a,e], Martin-Georg Endress[a], and Jonathan L. Payne[f]

Edited by James Brown, University of New Mexico, Morro Bay, CA; received January 24, 2022; accepted May 11, 2022

Rising temperatures are associated with reduced body size in many marine species, but the biological cause and generality of the phenomenon is debated. We derive a predictive model for body size responses to temperature and oxygen (O_2) changes based on thermal and geometric constraints on organismal O_2 supply and demand across the size spectrum. The model reproduces three key aspects of the observed patterns of intergenerational size reductions measured in laboratory warming experiments of diverse aquatic ectotherms (i.e., the "temperature-size rule" [TSR]). First, the interspecific mean and variability of the TSR is predicted from species' temperature sensitivities of hypoxia tolerance, whose nonlinearity with temperature also explains the second TSR pattern—its amplification as temperatures rise. Third, as body size increases across the tree of life, the impact of growth on O_2 demand declines while its benefit to O_2 supply rises, decreasing the size dependence of hypoxia tolerance and requiring larger animals to contract by a larger fraction to compensate for a thermally driven rise in metabolism. Together our results support O_2 limitation as the mechanism underlying the TSR, and they provide a physiological basis for projecting ectotherm body size responses to climate change from microbes to macrofauna. For small species unable to rapidly migrate or evolve greater hypoxia tolerance, ocean warming and O_2 loss in this century are projected to induce >20% reductions in body mass. Size reductions at higher trophic levels could be even stronger and more variable, compounding the direct impact of human harvesting on size-structured ocean food webs.

temperature-size rule | ecophysiology | climate change | hypoxia | metabolic index

Significance

Warming of the ocean is predicted to cause a reduction in the body sizes of marine animal species, but the biological basis for this prediction remains debated. We present a generalized mechanistic model of oxygen supply and demand that successfully reproduces the magnitude, variation, and temperature and body size dependence of body size responses to temperature change in laboratory experiments, supporting oxygen limitation as their underlying cause. When applied to accelerating future climate change scenarios, our results imply that the "temperature-size rule" will cause widely varying responses across the body size spectrum from microbes to macrofauna, impacting the function of size-structured marine food webs.

Body size is an important trait for a variety of ecological and biogeochemical processes from predator–prey dynamics to carbon cycling. Across a wide range of taxa, body size varies with environmental temperature. From microbes to animals, species tend to grow larger in colder habitats both when comparing closely related species (1) and different populations within a species (2). Body size also decreases when temperatures rise on timescales from seasonal cycles (3) to paleoclimate transitions (4, 5). In natural settings, the role of temperature may be confounded by co-occurring environmental changes. Thus, a key to understanding body size changes across thermal clines in nature lies in laboratory rearing experiments that measure the effect of elevated temperature on the maximum body size of successive generations. Over 80% of ectotherm species grow to a smaller body size when reared under warmer conditions, a pattern termed the "temperature-size rule" (TSR) (6–8). The magnitude of the decrease in maximum body size averages ∼4%/°C but varies strongly among species of different sizes and, in some cases, across the experimental temperature range for a single species (Fig. 1*A* and *B* and *SI Appendix*, Fig. S1), providing valuable information about possible underlying mechanisms.

Among aquatic ectotherms, the TSR has been ascribed to limitation by dissolved O_2 (9, 10). According to this hypothesis, a thermally driven increase in O_2 demand outpaces any rise in O_2 supply, a balance that can be restored by confining growth to a smaller size, resulting in a larger ratio of respiratory surface area to body volume (9). Consistent with this hypothesis, compilations of experimental data show that aquatic taxa are more prone to O_2 limitation in warmer water (11–13) and have a stronger body size response to temperature than terrestrial taxa (7). However, the impact of body size on O_2 limitation itself is ambiguous (14). For fish, it has been argued that metabolic rates rise more quickly with body size than does gill surface area, but the relationship of both metrics to body size varies widely between species, and gill area is only an indirect measure of O_2 supply that does not take into account ventilation and perfusion. Intraspecific studies have revealed both increases and decreases in hypoxia tolerance as organisms grow, while comparisons of hypoxia tolerance across species of different body size show weak and/or insignificant trends (14, 15). Direct experimental support for the TSR is largely confined to small species (mass < 1 g), leaving its relevance for macrofauna such as fish highly uncertain and debated (16–18).

Author affiliations: [a]School of Oceanography, University of Washington, Seattle, WA 98105; [b]Department of Geosciences, Princeton University, Princeton, NJ 08540; [c]High Meadows Environmental Institute, Princeton University, Princeton, NJ 08540; [d]Department of Animal Ecology and Physiology, Radboud University, Nijmegen, 6500 GL Nijmegen,The Netherlands; [e]Department of Marine Science, University of Rhode Island, Narragansett, RI 02882; and [f]Department of Geological Sciences, Stanford University, Stanford, CA 94305

Author contributions: C.D. designed research; C.D. performed research; C.D., J. L. Penn, K.I., and M.E. analyzed data; and C.D., J. L. Penn, W.C.E.P.V., and J. L. Payne wrote the paper.

The authors declare no competing interest.

This article is a PNAS Direct Submission.

[1]To whom correspondence may be addressed. Email: cdeutsch@princeton.edu.

This article contains supporting information online at http://www.pnas.org/lookup/suppl/doi:10.1073/pnas.2201345119/-/DCSupplemental.

Published July 5, 2022.

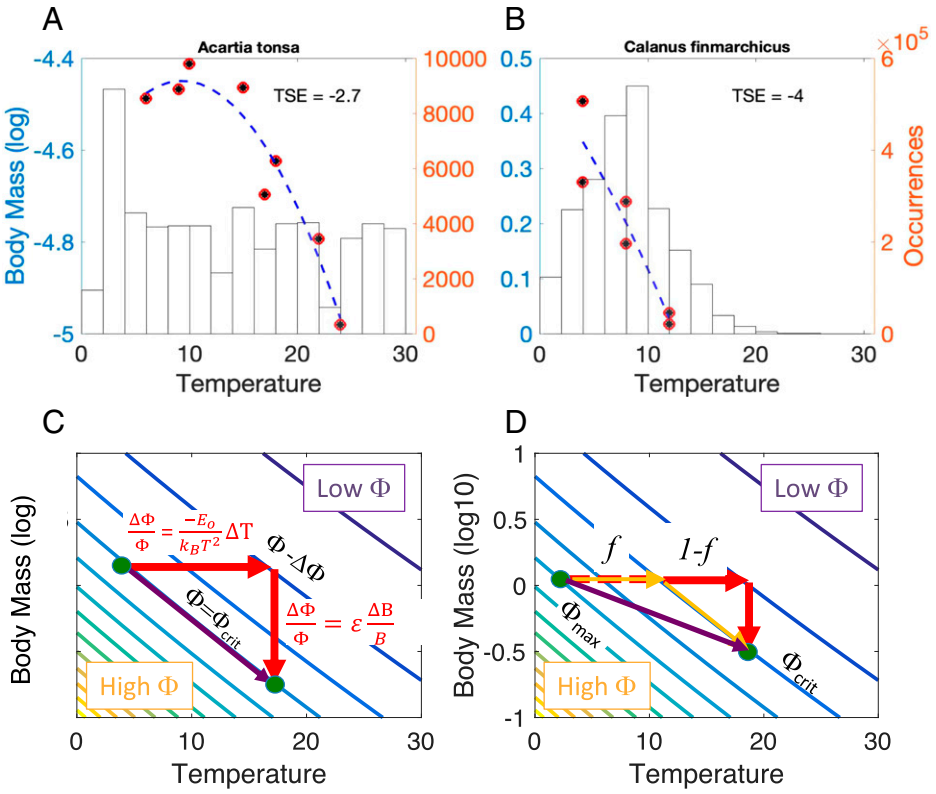

Fig. 1. Effect of temperature on body size. (*A* and *B*) Body size (log) versus temperature from rearing experiments for two species in data compilation used for model analysis (also *SI Appendix*, Fig. S1). The log(*B*) versus temperature data are fit with a quadratic curve (dashed) whose local slope is the fractional change in body size per degree (i.e., TSE, %/°C). The two species of zooplankton (44, 45) illustrate the tendency for the TSE to be stronger in warmer water (*B*) and among larger species (*B* vs. *A*). Bars indicate the number of times reported species locations map to each temperature bin in a global climatology (*Materials and Methods*). (*C* and *D*) Schematic model based on the metabolic index (isolines) of a hypothetical species with $E_o > 0$ and $\varepsilon < 0$ (see Eq. **1**). If tolerance for low O_2 declines at higher *T*, then warming reduces the metabolic index (horizontal arrows), which will reduce fitness and survival. If tolerance for low O_2 declines with size, then fitness can be restored by shrinking (vertical arrows). The magnitude of TSE for organisms already at their aerobic survival limit (*C*) will be greater than for those (*D*) that can accommodate a fraction, *f*, of the reduction in Φ by curtailing activity either prior to reducing body size (orange arrows) or simultaneous with it (purple arrow), yielding the same average size change per degree Celsius.

To evaluate the potential role of oxygen in generating temperature-size responses, a quantitative theory of how oxygen supply and demand change with temperature and body size is needed. Such a quantitative model should account for the apparent generality of the TSR across diverse taxonomic groups and aquatic environments and be able to predict the magnitude of the effect (hereafter, "temperature-size effect" [TSE]), its frequency distribution among species, its differences across the environmental temperature range, and within and across size classes. Here we present such a model based on the metabolic index (Φ), a measure of the ratio of O_2 supply to demand for aquatic ectotherms (12, 19–22).

A Mechanistic Model

The potential rate of oxygen supply from the environment and the resting rate of oxygen demand of an organism both depend on temperature (*T*) and body mass (*B*), and the ratio of these rates can be approximated by $\Phi = A_o \cdot pO_2 \cdot \left(\frac{B}{B_{ref}}\right)^{\varepsilon} \cdot exp\left(\frac{E_o}{k_B}\left(\frac{1}{T}-\frac{1}{T_{ref}}\right)\right)$ (12). Here, pO_2 is the ambient O_2 pressure (atm) and A_o (atm^{-1}) is a species-specific hypoxia tolerance, defined as the inverse of the lowest pO_2 that can sustain resting metabolic demand at a reference temperature (T_{ref} in kelvins) and body mass (B_{ref} in grams). The parameters, ε (unitless) and E_o (in electronvolts), define the sensitivity of hypoxia tolerance to body size and temperature, respectively, traits that also differ among species. Commonly observed allometric scaling of O_2 demand ($D \sim B^{\delta}$) and supply ($S \sim B^{\sigma}$) imply that their ratio (i.e., Φ) varies with body size to the power $\varepsilon = \sigma - \delta$. This exponent is negative when the supply/demand ratio decreases with size ("smaller is better," $\delta > \sigma$) and positive when it increases with size ("larger is better," $\sigma > \delta$). The temperature sensitivity of Φ, represented by E_o (and the Boltzmann constant, k_B), is also the difference between that of demand and supply. The value of E_o is positive when metabolic demand increases with temperature faster than O_2 supply ("colder is better"), but it can be negative when mechanisms of O_2 supply, such as circulation and ventilation, accelerate with temperature faster than metabolism, which is less rare in cold water (23). For animals in which the metabolic index declines with both temperature ($E_o > 0$) and body size ($\varepsilon < 0$), a warming-induced reduction in the aerobic capacity of the environment could be compensated by a reduction in body size.

The metabolic index traits defining hypoxia tolerance (A_o) and its temperature and allometric sensitivities (E_o and ε) have been estimated across a diverse array of marine species, using laboratory experiments in which O_2 declines to a critical pressure (P_{crit}) at which supply just balances resting demand and Φ reaches its resting lower limit of 1. However, metabolism at rest is insufficient for individual or population survival. To supply energy for growth and ecological activity, the threshold for long-term habitability must rise to values ranging from ~1.5 to 6, termed Φ_{crit}, corresponding to species-specific ratios of metabolic rates under sustained activity relative to the resting state (21).

For an organism in an environment where Φ is already at the lower limit for active, long-term survival ($\Phi = \Phi_{crit}$), a

reduction in Φ due to warming (if $E_o > 0$) could be compensated by reduced body size (if $\varepsilon < 0$). For a rise in temperature (ΔT), the fractional change in the environment's capacity to meet an organism's O_2 demand ($\Delta\Phi/\Phi$) is equal to $\frac{-E_o}{k_B T^2}\Delta T$ (Fig. 1*C*; horizontal red arrow). The same fractional change in Φ can be induced by a change in body size of magnitude $\varepsilon\frac{\Delta B}{B}$ (Fig. 1*C*; vertical red arrow). Maintaining constant Φ equates these quantities, yielding a simple expression for the fractional change in body size per degree of warming, the TSE: $\mathrm{TSE} \equiv \frac{1}{B}\frac{\Delta B}{\Delta T} = \frac{E_o}{\varepsilon k_B T^2}$ (Fig. 1*C*). Accordingly, size reductions should get stronger as either E_o becomes more strongly positive or as ε becomes less strongly negative. As the allometry of O_2 supply and demand converge, an increasingly large change in body size is needed to compensate for a given reduction in Φ.

In general, ambient pO_2 is greater than the minimum required for sustained survival (i.e., $\Phi > \Phi_{crit}$), allowing rates of activity to approach maximum physiologically achievable levels. Active metabolic rates in fish peak at ∼3 to 12 times those at rest (24), but only when Φ is likewise 3 to 12, a value we denote by Φ_{max}. A fraction (f) of the warming-induced reduction in Φ may be accommodated by curtailing the highest rates of activity, partially alleviating the need for body size reduction (Fig. 1*D*). In such cases, the TSE is simply scaled by $1-f$. Moreover, in natural environments, temperature changes are usually accompanied by changes in pO_2 that would ameliorate (if pO_2 increases with T, i.e., $\frac{\Delta pO_2}{\Delta T} > 0$) or exacerbate (if pO_2 decreases under warming, $\frac{\Delta pO_2}{\Delta T} < 0$) the thermal decline in Φ. These two modifications yield a simple predictive equation for the TSE (for a detailed mathematical derivation, see *SI Appendix, Methods*):

$$TSE = \frac{1}{B}\frac{\Delta B}{\Delta T} = \frac{(1-f)}{\varepsilon}\left\{\frac{E_o}{k_B T^2} - \frac{1}{pO_2}\frac{\Delta pO_2}{\Delta T}\right\}. \quad [1]$$

In principle, this model allows the TSE measured in laboratory rearing experiments across multiple generations to be predicted from short-term respirometry data. In practice, experimentally derived TSE and respirometry are rarely available for the same species. However, the model can be tested statistically by comparing frequency distributions and trends in observed TSE values to those predicted from distributions of metabolic index parameters. We compiled datasets from published literature to estimate the key parameters (E_o, ε, and f) and compared the model-predicted TSE to experimental values (*Materials and Methods*). We also evaluated the relationship between allometric exponents ($\varepsilon = \sigma - \delta$) using values derived from both ontogenetic (within-species) and phylogenetic (between-species) variation in O_2 supply and demand. All reported relationships are statistically significant based on tests and statistics described in the referenced *SI Appendix*, Figs. S1–S7 and Table S2.

Trait-Based Predictions

The temperature sensitivity of the metabolic index varies widely across species, from $E_o = -0.2$ to +1.1 eV (19, 21). A preponderance of positive values indicates that the O_2 supply/demand ratio of most species decreases with temperature (colder is better) yielding a factorial loss of aerobic capacity $\left(\frac{E_o}{k_B T^2}\right)$ from warming (Fig. 2*A*), whose magnitude and variability (interquartile range, 2.6 to 7.9%/°C) is comparable to factorial size reductions observed in laboratory data (*SI Appendix*, Fig. S1). The decline of hypoxia tolerance from warming also tends to become more acute as temperatures rise so that E_o increases with temperature (21) (*SI Appendix*, Fig. S2*A*). In some species, hypoxia tolerance has an optimum temperature (23, 25), below which hypoxia tolerance also decreases in cold water ("warmer is better," $E_o < 0$). However, for large temperature increases applicable to rearing experiments, most species will face a substantial loss of aerobic scope as measured by the median 4.8%/°C decline in Φ.

If the initial Φ in an environment is above Φ_{crit}, then the total loss of aerobic capacity can be partly accommodated by simply decreasing peak activity levels, thus buffering populations from the need to reduce body size. To evaluate this activity buffer factor (f), we compared the values of Φ_{crit} that define the lower limits of habitability to the highest values (Φ_{max}) found in each species geographic range (i.e., $f = 1 - \Phi_{crit}/\Phi_{max}$; *Materials and Methods*). Across all 37 species with both distributional and trait data, we find that these minimum thresholds for habitability are on average ∼1/2 as large as the highest values encountered in the species geographic range, with variation not related to body size (Fig. 2*B* and *SI Appendix*, Fig. S2*B*). The value of Φ_{crit} has also been shown to correspond to an energy provisioning nearly half that required for a species to achieve its maximum metabolic rate (21). These findings both imply that for most species, aerobic scope can be reduced to ∼50% of that needed for peak performance before the threshold for survival (Φ_{crit}) is reached.

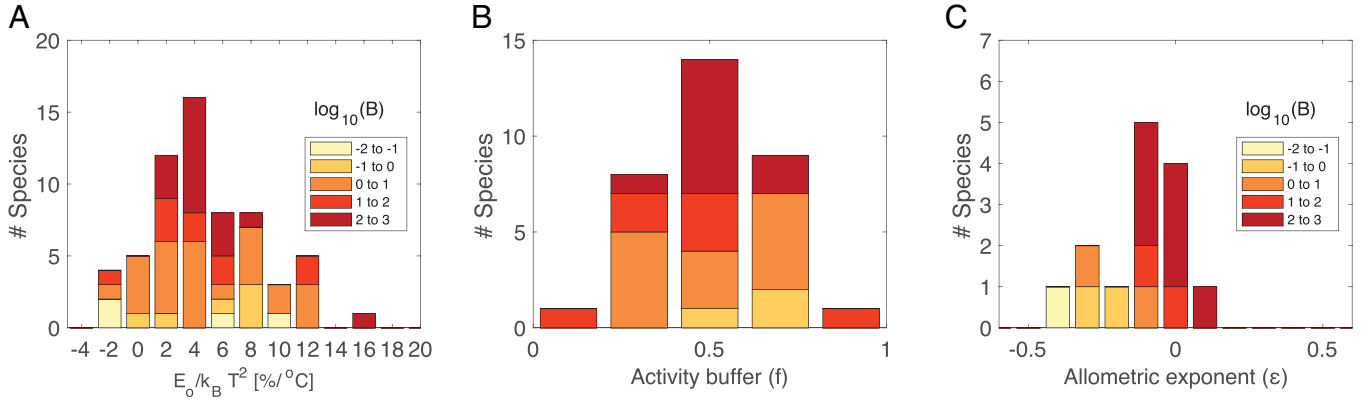

Fig. 2. Empirically derived components of the predictive model for TSE. (*A*) Fractional change in metabolic index per degree of temperature change among 72 species for which E_o has been measured. (*B*) Activity buffer (f), estimated from the minimum and maximum values of Φ (i.e., Φ_{crit} and Φ_{max}, respectively) within each species' current geographic range as $f = 1 - \Phi_{crit}/\Phi_{max}$ (*Materials and Methods*). (*C*) Hypoxia tolerance versus body size for 14 species, measured as the allometric exponent (ε) for the body size dependence of P_{crit}. All histograms are colored according to median experimental body mass ($\log_{10}$ in grams) of each species.

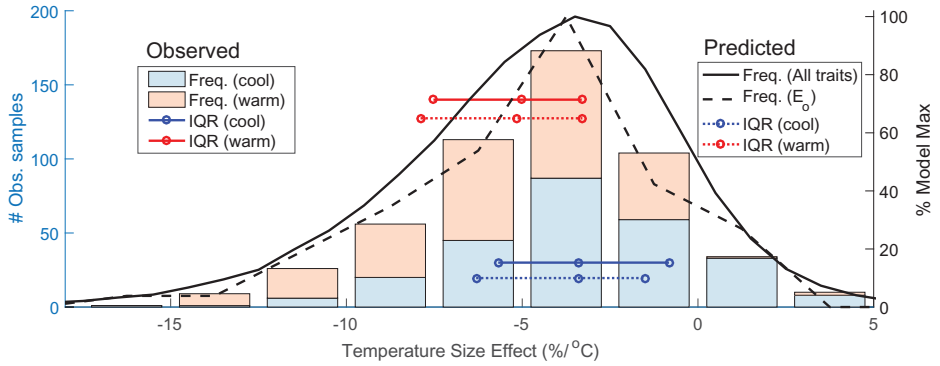

Fig. 3. Observed versus predicted TSE and its variations across the temperature range. The relative change in body size per degree of temperature change (TSE, %/°C) measured in laboratory rearing experiments varies widely among species and across temperature (bars; *Left* axis). The observed distribution is statistically indistinguishable (*SI Appendix*, Table S2) from that predicted by metabolic index model (lines; *Right* axis) based on the diversity of physiological traits (solid curve; see Fig. 2), but driven primarily by the temperature sensitivity of hypoxia tolerance E_o (dashed curve). Within distinct temperature ranges, the magnitudes of TSE (quartile markers on horizontal line segments) are significantly higher in water warmer than the median experimental temperature (red bars and lines) than in waters below that temperature (blue bars and lines), in both observations (solid line segments) and in model predictions (dashed line segments). The metabolic index model reproduces the direction and magnitude of this difference because the temperature sensitivity of hypoxia tolerance is significantly greater at warmer temperatures (*SI Appendix*, Table S2). Freq, frequency; IQR, interquartile range; Obs, observed.

As organisms grow, their hypoxia tolerance can change but the ontogenetic relationship between hypoxia tolerance and body size (ε) is less well established than its variation with temperature (E_o). Among the 14 species for which P_{crit} was measured across at least a twofold range of body size (*SI Appendix*, Table S1), larger individuals exhibited slightly lower tolerance to hypoxia, indicating that O_2 demand increased with size slightly faster than did O_2 supply. Indeed, the mean ontogenetic exponent across species (Fig. 2*C*) is significantly below zero ($\varepsilon = -0.12$; *SI Appendix*, Table S2) and is also significantly correlated with body size (*SI Appendix*, Fig. S2*C* and Table S2), increasing from the most negative exponents among the smallest species to values near zero among larger-bodied animals (Fig. 2*C* and *SI Appendix*, Fig. S2*C*).

The frequencies of these key physiological traits (E_o, f, and ε) can be used to predict the magnitude and variability of the TSE observed across species, body sizes, and temperatures. Monte Carlo simulations across species traits yield a frequency distribution of TSE (Fig. 3*A*, lines) that is statistically indistinguishable from experimental values (Fig. 3*A*, bars; *SI Appendix*, Table S2). The range of TSE magnitudes due to variability in all traits (Fig. 3*A*, solid line) derives primarily from the interspecific differences in the temperature sensitivity of hypoxia tolerance (E_o) (Fig. 3*A*, dashed line). While the variability in TSE magnitude among species can largely be accounted for by these interspecific variations in E_o, smaller variations in TSE across temperature and body size provide further tests of the trait-based model.

Laboratory data reveal a significantly stronger TSE on the warm side of the median experimental temperature than on the cold side (mean ΔTSE 2.5%/°C; *SI Appendix*, Table S2). This difference is consistent with changes in the hypoxia temperature sensitivity, which is also greater in warmer than in colder water (mean $\Delta E_o = 0.2$ eV; *SI Appendix*, Fig. S2*A* and Table S2) (21). Moreover, the distinct temperature sensitivities on the warm versus cool side of median experimental temperatures predict significantly different modeled distributions of the TSE that are each indistinguishable from the corresponding TSE observations under both warm and cool conditions (Fig. 2*C* and *SI Appendix*, Table S2). Thus, the tendency of rising temperature to induce an accelerated decline in hypoxia tolerance also leads to ever-stronger reductions in body size across generations.

Compilations of empirical TSE have also revealed stronger size reductions with warming among larger aquatic ectotherm species (7). The model reproduces the observed trend toward increasing TSE magnitude with increasing size (Fig. 4). This trend cannot be explained by a size dependence of the temperature sensitivity (E_o) or by the aerobic buffer (f), which have no significant relationship to body size among investigated species (Fig. 2). Nor can it be attributed to an O_2 supply-to-demand that scales isometrically with surface area versus volume, as such geometric arguments imply a constant ε and thus a constant TSE across the size range. Instead, the increased TSE among larger species requires that the allometric scaling of hypoxia tolerance (i.e., ε) itself varies with body size, as observed here (*SI Appendix*, Fig. S2). As the metabolic index becomes less size dependent for larger species and the absolute values of ε become smaller, a larger change in body size is needed to restore the loss of aerobic energy balance.

In summary, the widely variable TSE across species primarily reflects the diverse temperature sensitivities of hypoxia tolerance, whose nonlinear temperature dependence also explains the increase in TSE with warming. In contrast, the observed increase in TSE with body size is driven by a declining size dependence of hypoxia tolerance, which may be achieved either by O_2 demand becoming less size dependent (δ getting smaller) or O_2 supply becoming more dependent on size (σ getting larger). To diagnose the underlying causes of convergent trends in the body size dependence of O_2 supply and demand rates, we developed a model that combines theoretical and empirical allometric scaling across the full body size spectrum from microbes to large animals.

Allometry of Hypoxia Tolerance

Across multiple phyla, metabolic rates are related to body size with an approximate power law, B^{δ} (26, 27) (Fig. 5*A*). However, the exponent itself varies with body size (28), declining from $\delta \sim 1$ for small protists to $\delta \sim 3/4$ for large metazoans (Fig. 5*B*). These phylogenetic slopes (δ_{phy}) are consistent with the ontogenetic slopes (δ_{ont}) measured in various fish species (median $\delta_{ont} = 0.81$; interquartile range, 0.74 to 0.91), although the latter vary widely (24, 29).

The allometric scaling of O_2 supply (σ) is not directly measurable but can be evaluated indirectly from theory and respirometry data. At the smallest end of the size spectrum, aerobic microbes obtain O_2 through the body surface area, which scales with $B^{2/3}$, while the boundary layer thickness over which O_2

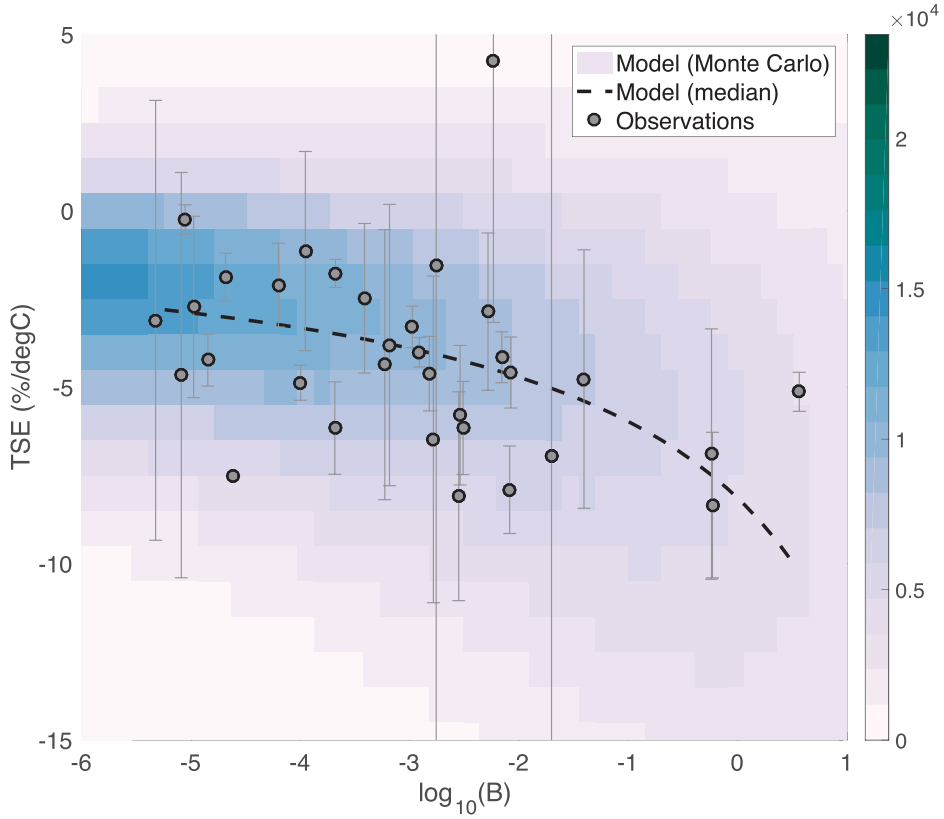

Fig. 4. Observed and predicted TSE and its variations across body size range. At each body size, variance in TSE is computed from the variability in species traits (E_o, f, and ε) via Monte Carlo simulation. The model predicts a nonlinear increase in both the mean magnitude and variation in TSE for larger body sizes because ε increases toward zero at larger sizes and TSE ~ 1/ε. Error bars on the observations represent the SD of TSE across the range of experimental temperatures (e.g., *SI Appendix*, Fig. S1).

must diffuse also increases with size ($B^{1/3}$), so that the diffusive supply should vary as $\sigma \sim 1/3$. Among macrofauna, the allometry of O_2 supply evaluated from interspecific respirometry data (*Materials and Methods*) yields a value of $\sigma_{phy} = 0.66$ (CI, 0.57 to 0.74; *SI Appendix*, Fig. S3) consistent with that derived from indirect measures of O_2 supply based on gill geometry across species ($\sigma_{phy} = 0.71$; ref. 30) (Fig. 5 *A* and *B*).

As body size increases from unicells to macrofauna, the decrease in δ and the increase in σ would each contribute to ε becoming less negative (since $\varepsilon = \sigma - \delta$), such that hypoxia tolerance becomes less size dependent in larger species. This trend is qualitatively consistent with the available data on the body size dependence of hypoxia tolerance (Fig. 2*C* and *SI Appendix*, Fig. S2*C*).

To make a quantitative comparison between modeled and observed ε trends, we modeled the transition from the weak body size dependence of O_2 supply expected for microbes ($\sigma \sim 0.3$) to the strong size dependence inferred among large animals ($\sigma \sim 0.7$), by combining theoretical scaling with empirical constraints across the entire range of body sizes (*Materials and Methods* and *SI Appendix*, *Methods*). Despite variation across >10 orders of magnitude in body size, fluid flow at the sites of O_2 exchange remains laminar, allowing mass transfer rates to be derived from diffusive boundary layer scaling (31). The model predicts an increase in σ with body size, from $\sigma = 1/3$ for unicells to the empirically constrained $\sigma \sim 0.7$ at the largest sizes (Fig. 5*B*, blue line). This transition arises from an increase in the number, dimensions, and fluid velocity at the sites of O_2 exchange, which all increase with body size (details in *Materials and Methods*). The dependence of these parameters on body size is consistent with available compilations of gill morphometrics (*SI Appendix*, Fig. S4) and yields a σ largely independent of temperature (*SI Appendix*, Fig. S5). The free parameters that best match the directly measured ε data independently place the largest shift in σ at body masses of 0.1 to 10 g. Interestingly, this size range corresponds to the transition from animals that extract O_2 via their skin to those having gills or other respiratory organs.

Combining the allometric exponents of O_2 supply and demand yields a prediction for how hypoxia tolerance varies with body size (ε), across organisms spanning >10 orders of magnitude in body mass. Among unicellular microbes, modeled ε takes on large, negative values, due to both a relatively high δ and small σ. With increasing body mass, modeled ε becomes less negative, approaching 0, driven by both the declining size dependence of O_2 demand (i.e., δ) and by the increasing size dependence of O_2 supply (i.e., σ) of larger animals. The predicted ε values are consistent with independent empirical estimates from two microbial taxa (ciliates and dinoflagellates; Fig. 5*C*, triangles) and a planktonic copepod in the size range of the TSR experiments (*Calanus finmarchicus*; Fig. 5*C*, gray circle), the sole species for which TSE, E_o, and f are all available (*Materials and Methods*). Among larger species, modeled variations in ε reproduce the trends observed in the direct ontogenetic estimates from laboratory respirometry (Fig. 5*C*).

The ontogenetic change in hypoxia tolerance averaged across the available species ($\varepsilon_{ont} = -0.12$) matches that derived from phylogenetic variation, as estimated from body size dependence of temperature-normalized hypoxia tolerance (A_o) across species ($\varepsilon_{phy} \sim -0.13 \pm 0.18$ SE; *SI Appendix*, Fig. S3*C*). This finding suggests that allometric scaling derived from interspecific relationships approximates mean ontogenetic effects averaged across species. In the only available study to date of hypoxia tolerance spanning multiple orders of magnitude in body size within a

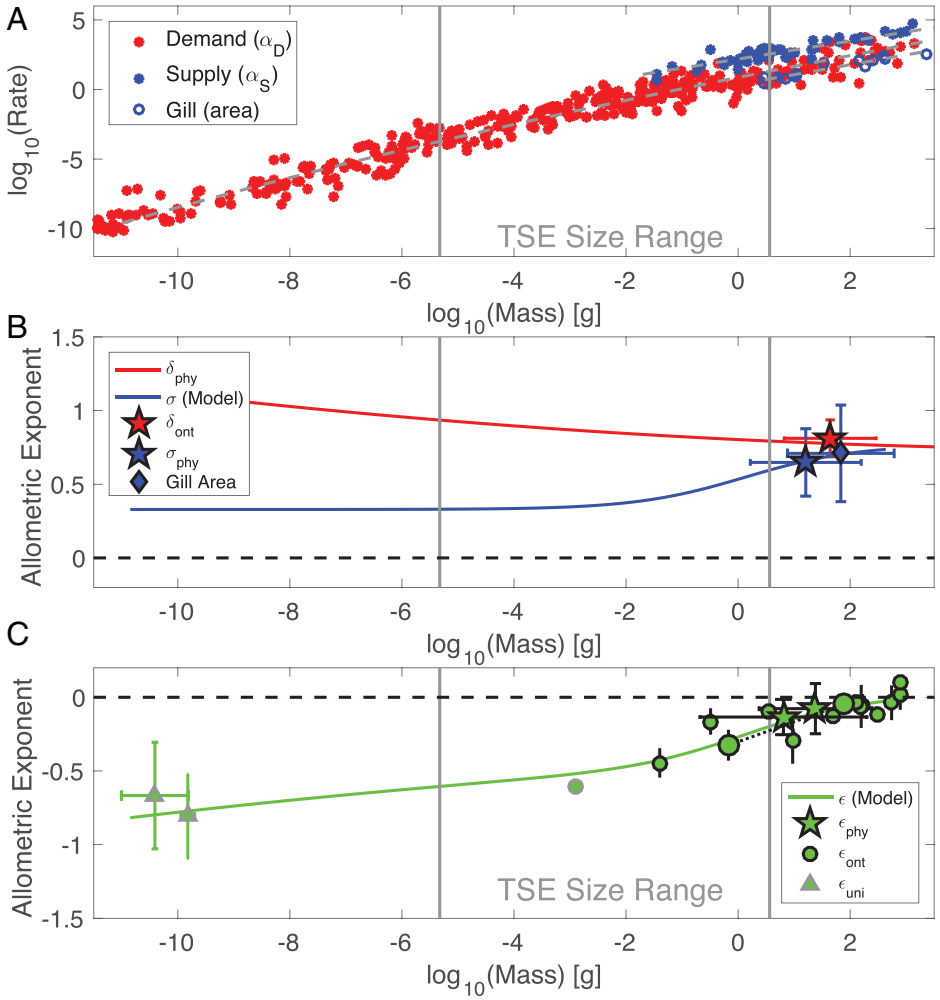

Fig. 5. Variation of O_2 supply and demand, and their allometric scalings, across body sizes from unicells to macrofauna. (*A*) Resting metabolic O_2 demand (α_D; red points) and O_2 supply rate coefficients (α_S; blue points) estimated at a reference body size and temperature from respirometry (solid; ref. 21) and from gill morphometric data (open; ref. 30). (*B*) The allometric exponents characterizing variations in supply and demand versus size are derived from slopes of the log-log plot (*A*), with ontogenetic estimates within species (markers). (*C*) The difference between allometry of supply and demand versus body size using the individual curves (*B*) with empirical estimates (*Materials and Methods*) from animals and unicells (markers). Markers outlined in black indicate estimates based directly on measured P_{crit}, those outlined in gray are indirect estimates (unicells and *C. finmarchicus*; *Materials and Methods*), and larger circles connected by dotted line are separate ε estimates from the same species (red drum) where P_{crit} was measured across approximately three orders magnitude in body size (32). Phylogenetic exponents from P_{crit} trends with body size (i.e., ε_{phy}; stars) also increase when estimated across only larger species ($B > 1$ g), relative to estimates from all available species (*SI Appendix*, Fig. S3).

single species (red drum; ref. 32), measured P_{crit} reveals a decline in hypoxia tolerance with size ($\varepsilon < 0$) that is significantly stronger for smaller animals ($\varepsilon = -0.32 \pm 0.1$ SE for $B < 10$ g) than for larger ones ($\varepsilon = -0.04 \pm 0.02$ SE for $B > 10$ g) (Fig. 5*C*; thin black dashed line). Similarly, the phylogenetic variation in temperature-normalized hypoxia tolerance (A_o) indicates a slightly weaker allometric dependence when restricted to only the larger size classes ($\varepsilon_{phy} \sim -0.08$ for $B > 1$ g; *SI Appendix*, Fig. S3*C*). The available data thus support consistent phylogenetic and ontogenetic trends in ε across the size spectrum, mirroring the findings for metabolic rates ($\delta_{ont} \sim \delta_{phy}$). Despite these broad trends, allometric scaling exponents can be highly variable within a given size class, including cases with ontogenetic increases in hypoxia tolerances ($\varepsilon > 0$) among larger animals (Fig. 2*C*; 14).

Implications for Climate and Food Webs

Using this empirically validated model, we estimated the impact of climate changes in ocean temperature and O_2 projected for the end of the century by Earth system models if greenhouse gas emissions continue to accelerate (Fig. 6). For a typical temperature sensitivity ($E_o = 0.4$ eV) and allometric exponent of $\varepsilon = -0.3$ expected for small-bodied species at the base of the food web ($B \sim 1$ g), warming and deoxygenation of the upper ocean would yield reductions in body mass of 10 to 30%, with larger magnitudes in northern oceans where warming and O_2 loss are stronger (Fig. 6*A*).

Body size reductions may ameliorate the loss of aerobic habitat and thus the risk of extirpation (33). However, if warming proceeds unchecked and the efficacy of adaptive or migratory strategies is limited, total size changes may eventually exceed some species' anatomically or ecologically viable size limits, resulting in extinction (Fig. 6 *B* and *C*). The magnitude of climate change required to precipitate such outcomes varies strongly across the range of measurable species traits. Large fractional size reductions are more likely for species whose hypoxia tolerances are only weakly size dependent, a condition that characterizes most macrofauna (Fig. 6*B*), or for those species more sensitive to temperature (Fig. 6*C*).

Although the mechanism underlying these reductions is aerobic metabolism, the dominant driver of size reductions within this century is the rise of temperature and not the decline of pO_2 (*SI Appendix*, Fig. S6). On the multigenerational time scales

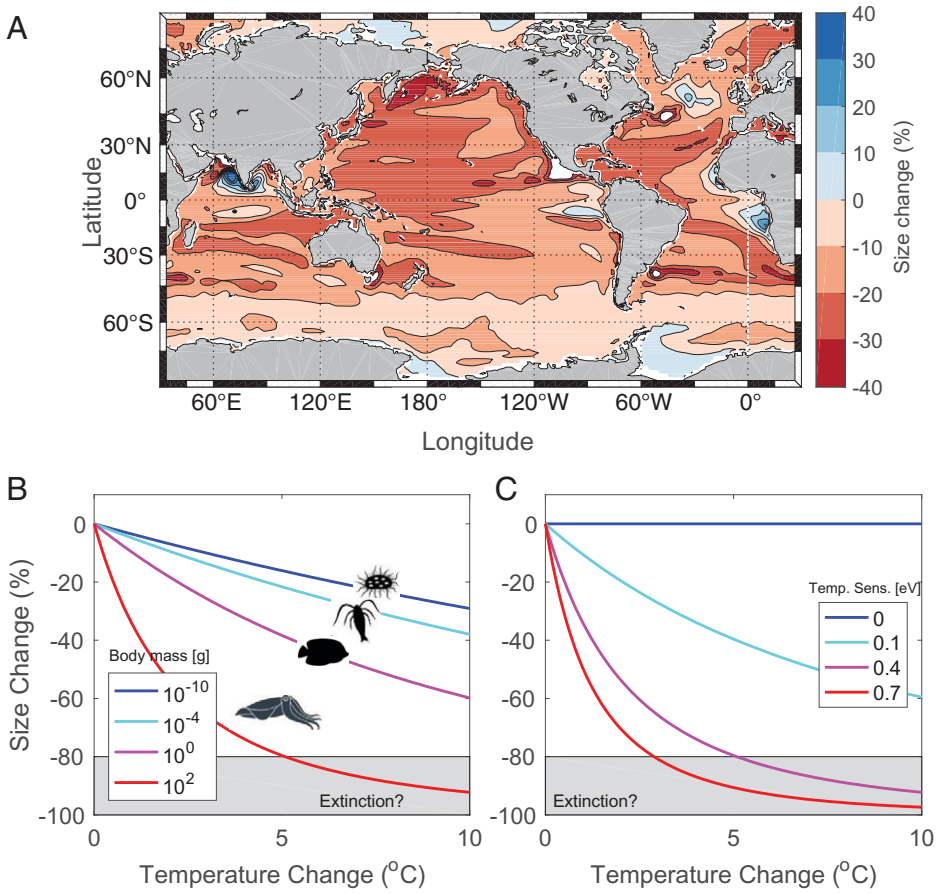

Fig. 6. Change in body size (%) over this century based on the mechanistic data-constrained model, and projected climate trends in temperature and O_2 from Earth system models. (*A*) Fractional change in body size for a 1-g water breather with $\varepsilon = -0.3$ and temperature sensitivity of $E_o = 0.4$ eV, for ocean climate changes in 2100 CE over the upper 500 m. (*B* and *C*) Changes in body size as temperatures rise, across a range of traits governing the (*B*) allometry and (*C*) temperature sensitivity of hypoxia tolerance. The body sizes in *B* correspond to representative species within the dataset (silhouettes) that exhibit distinct allometric exponents (ε) as shown in Figs. 2*C* and 5*C*.

of anthropogenic climate trends, adaptive evolution of traits could ameliorate these predictions. The complete model derivation (*Materials and Methods*) includes the potential evolution of hypoxia-related traits (*SI Appendix*, *Methods*), but the experimental data needed to estimate those responses are currently lacking.

Conclusions

The consistency between our mechanistic model and independent laboratory observations of the magnitude, variability, and trends in TSE provides strong support for the hypothesis that the temperature and size dependence of hypoxia tolerance is the primary driver of this widespread phenomenon. The size dependence of hypoxia tolerance could act through direct O_2 limitation of growth (a proximate cause) or via the evolution of thermal reaction norms that avoid such limitation (i.e., an ultimate cause) (10). The robust and consistent trends in allometric scaling of O_2 supply, O_2 demand, and the resulting hypoxia tolerance revealed across the full spectrum of body sizes have broad implications for body size responses to temperature, which extend beyond the scope of direct experimental TSE data.

Our model helps reconcile divergent views on whether a warming ocean will cause a shrinking of fish and other macrofauna for which the TSE has not been directly observed. The core assumption of the predicted shrinkage, that O_2 demand increases with body size faster than does O_2 supply (16, 17), has been questioned on the physiological grounds that $\varepsilon \sim 0$ (14, 18), implying that growth is not O_2 limited. Our analysis supports both contentions by demonstrating that while O_2 limitation is prevalent among smaller species ($\varepsilon < 0$), it gradually gives way to close allometric coupling of supply and demand ($\varepsilon \sim 0$) among larger-bodied animals. However, the model predicts—and available data support—that as ε rises toward zero, the size response to temperature becomes stronger, not weaker. Thus, species whose O_2 supply and demand is closely but not exactly balanced may still exhibit an aerobically driven reduction of body size in response warming or O_2 loss, unless superseded by other physiological or anatomical constraints.

The physiological responses of animal body size to ocean warming and deoxygenation will also be modulated by ecological processes. The ability of some populations to avoid reduced Φ by tracking preferred thermal and aerobic conditions through migration may make body size reductions a less important response to climate change (20, 34) and may be more feasible for larger animals. However, even species with strong migratory capacity will likely feed on prey species of smaller size, impacting body size indirectly through the food web. Changes in the body mass of individual organisms summed across species also have the potential to directly alter the biomass of the entire food web, especially at higher trophic levels. Interestingly, global biomass losses of a comparable magnitude (~5%/°C) and with a similar trophic amplification have been projected by ecosystem models due to reduced primary productivity (35), but a contribution of the TSE to such projections remains to be quantified.

Our model predictions are also consistent with fossil evidence indicating preferential extinction of larger species, and of size

reduction within survivors, across past extinction events associated with global warming and ocean deoxygenation (5, 36–39). The wide variability in temperature sensitivity of hypoxia tolerance will modulate this pattern (Fig. 6*C*), allowing some large species to persist and smaller species to perish, potentially underpinning the variation in extinction seen within fossil size classes. Whether extinction thresholds are crossed this century, the exponential nature of size responses and their disproportionate impact on larger animals implies an early and substantial contraction and reorganization of size-structured marine food webs and the carbon cycling they affect. This indirect climate impact would exacerbate ongoing anthropogenic selection against large marine fauna due to hunting and overfishing (40, 41) that has already left detectable fingerprints on marine ecosystems over the past century.

Materials and Methods

Predictive Model. To derive the relationship between body size, environmental change, and species traits, we begin with the metabolic index (Φ) defined as the ratio between rates of potential O_2 supply (S) driven by its ambient pressure (pO_2) and the resting oxygen demand by the organism (D) both of which depend on temperature (T) and body mass (B): $\Phi = \frac{S(B,T)}{D(B,T)} = A_o \cdot pO_2 \cdot \left(\frac{B}{B_{ref}}\right)^{\varepsilon} \cdot exp\left(\frac{E_o}{k_B}\left(\frac{1}{T} - \frac{1}{T_{ref}}\right)\right)$. As detailed in earlier work (12, 19, 21), A_o represents a species' hypoxia tolerance (atm^{-1}), which varies with body mass (B) according to a power law, and exponentially with inverse temperature (Arrhenius function) with allometric and thermal sensitivities, ε and E_o, respectively.

Taking the logarithmic derivative of Φ with respect to temperature and rearranging terms, we derive a predictive equation (details in *SI Appendix, Methods*) for the intergenerational response of body size to temperature:

$$\mathrm{TSE} = \frac{\partial ln(B)}{\partial T} = \frac{(1-f)}{\varepsilon}\left\{\frac{E_o}{k_B T^2} - \frac{\partial \ln(pO_2)}{\partial T}\right\} - \frac{1}{\varepsilon}\left\{\frac{\partial ln A_o}{\partial T} + c\frac{\partial E_o}{\partial T}\right\},$$

where the TSE is defined as the fractional change in body mass per degree of temperature, a common experimental metric. Absent evolutionary changes, which are quantified by the last term on the right hand side, the parameters needed to predict the TSE can be obtained from respirometry (21), with the exception of the buffer factor (f), which is estimated from biogeographic data (see below).

Species Traits. We used laboratory observations of body mass across a range of experimental temperatures compiled by Forster et al. (7). To maximize data, we included both freshwater and marine species, which show similar temperature-size responses. The TSE can be measured as the slope of the relationship between the natural log of body mass versus temperature. However, some species exhibit a nonlinear relationship (*SI Appendix*, Fig. S1), implying that the TSE itself varies in strength across the temperature range. To account for this nonlinearity, we instead fit ln(B) to a quadratic function of temperature, the lowest-order polynomial that allows for estimation of significant differences in TSE between cooler and warmer waters. We discard species for which this quadratic curve accounted for less than 25% of the variance in the data (i.e., Pearson correlation coefficient, $r^2 < 0.25$), yielding 33 species. The TSE at each temperature is then computed from the fractional change in B at each temperature–that is, the slope of the ln(B) versus T curve. The histogram of TSE estimated at each temperature for all species is shown as the number of samples (Fig. 3*A*, bars), while a single TSE for each species was computed from the intraspecific mean value across all temperatures (Fig. 4, markers).

To predict the magnitude and variance of TSE, we used data recently compiled on the temperature and size dependence of the O_2 supply and demand of marine species (21). Because the critical threshold for O_2 limitation at rest is given by the ratio of O_2 supply and demand (i.e., Φ) rather than by either rate individually, the most useful parameters are those that measure a threshold value of this ratio (i.e., the critical oxygen threshold, P_{crit}) versus either body size (ε) or versus temperature (E_o). We obtained estimates of E_o from 72 species, while our literature search for data to estimate ε yielded values for 14 species. To facilitate comparison of the TSE measurements on smaller body sizes, we used the species estimates of ε to calibrate a theoretical model that spans the full range of body mass (see below).

To evaluate the aerobic activity buffer, which can be approximated as $f \sim 1 - \frac{\Phi_{crit}}{\Phi_{max}}$ (*SI Appendix, Methods*), we determined the upper and lower limits of Φ from each species habitat for which both metabolic index traits and a well-sampled geographic range are available. The geographic range is based on occurrences reported in the Ocean Biodiversity Information System database (https://www.obis.org/) and its matching to hydrographic conditions in the World Ocean Atlas is described in Deutsch et al. (21). Temperatures in TSE experiments span similar gradients to those found across each species' natural range (Fig. 1*A*, *Insets*, and *SI Appendix*, Fig. S1), indicating that the buffer factor derived from biogeographic data should also be applicable in a laboratory setting. For any given species, TSE experiments may be initiated above or below the temperature at which Φ_{max} is achieved. However, we see no reason to expect a systematic bias across all species, and we therefore take the mean value of the slope of Φ_{crit} versus Φ_{max}, a representative value of f applicable to all species. Indeed, the value of f based on ratios of Φ_{crit}/Φ_{max} yields similar results to the ratio of sustained to maximum metabolic rates (MMRs) analyzed by Deutsch et al. (21), indicating that the maximum Φ in a species' habitat is that which supports its MMR, an outcome that may reflect evolutionary selection for O_2 supply capacity (15).

O_2 Supply Allometry. Across body sizes from unicells to large fish, we can compute the O_2 supply rate (S) using a model of diffusive boundary layer scaling as follows (*SI Appendix, Methods*):

$$S = [4\pi\, \kappa^* pO_2]\; Sh \cdot r_e \cdot n_e.$$

Body size influences this supply rate explicitly through the number (n_e) and size of exchange elements (r_e) and implicitly through the effect of the Sherwood number (Sh; *SI Appendix, Methods*), which depends on r_e as well as on the fluid velocity at the exchange element (U_e). We assume that each of these factors (r_e, U_e, n_e) scales with biomass according to power law relationships: $n_e = n_o B^{n_1}$, $U_e = u_o B^{u_1}$, and $r_e = r_o B^{r_1}$. The allometric exponent of O_2 supply follows from the exponents in the power laws relating body size to the linear size (r_1), number (n_1), and fluid flow (u_1) at exchange element sites. The values of these parameters giving the best fit to ε observations were found to be $r_1 = 0.25$, $n_1 = 0.06$, and $u_1 = 0.73$, which compare favorably to empirical estimates of $r_1 = 0.27$ based on lamellar area (*SI Appendix*, Fig. S4), and the number of secondary lamellae among multiple species of sharks ($n_1 = 0.04$; ref. 42). The velocity exponent, $u_1 \sim 3/4$, implies that flow speed at the gill and whole organism metabolic rate increase at similar rates with body size, a finding that appears sensible but awaits empirical testing with new measurements and/or new compilations of existing data (*SI Appendix, Methods*).

Climate Projections. We used Earth system model projections of future climate states to compute changes in temperature and pO_2 at the end of the 21st century. The model runs were performed for the fifth assessment report of the Intergovernmental Panel on Climate Change, and results archived for the corresponding Climate Model Intercomparison Project (CMIP5). All model fields were interpolated to a 1° latitude/longitude grid with 33 depth levels for analysis. Climate anomaly fields for temperature and O_2 were constructed by subtracting monthly climatologies in 2071 to 2100 from monthly values in 1971 to 2000 for each model under the greenhouse gas emission scenario RCP8.5. To compute fractional change in pO_2 (per Eq. **1**), the pO_2 anomaly fields were divided in each grid cell by the climatological values in the 2018 World Ocean Atlas.

Data Availability. The MATLAB code is available in GitHub (https://github.com/cadeutsch/Temperature_Size_Rule_Metabolic_Index) (43). All other study data are included in the article and/or *SI Appendix*.

ACKNOWLEDGMENTS. We gratefully acknowledge the laboratory scientists whose data made this study possible, the international modeling centers that contribute to the archive of Earth system model output maintained by the Intergovernmental Panel on Climate Change through the CMIP, and Hartmut Frenzel, Andrew Mandovi, and Ella Cedarholm for assistance in data collection and curation. This work was made possible by grants from the Gordon and Betty Moore Foundation (GBMF#3775), NSF (OCE-1419323 and OCE-1458967), National Oceanic and Atmospheric Administration (NA18NOS4780167), and California SeaGrant and Ocean Protection Council.

1. S. F. Timofeev, Bergmann's principle and deep-water gigantism in marine crustaceans. *Izv. Akad. Nauk Ser. Biol.* **28**, 764–768 (2001).
2. F. C. James, Geographic size variation in birds and its relationship to climate. *Ecology* **51**, 365–390 (1970).
3. C. R. Horne, A. G. Hirst, D. Atkinson, Seasonal body size reductions with warming covary with major body size gradients in arthropod species. *Proc. Biol. Sci.* **284**, 20170238 (2017).
4. G. Hunt, K. Roy, Climate change, body size evolution, and Cope's rule in deep-sea ostracodes. *Proc. Natl. Acad. Sci. U.S.A.* **103**, 1347–1352 (2006).
5. J. L. Payne, Evolutionary dynamics of gastropod size across the end-Permian extinction and through the Triassic recovery interval. *Paleobiology* **31**, 269–290 (2005).
6. D. Atkinson, "Temperature and organism size–A biological law for ectotherms?" in *Advances in Ecological Research*, M. Begon, A. H. Fitter, Eds. (Academic Press, 1994), pp. 1–58.
7. J. Forster, A. G. Hirst, D. Atkinson, Warming-induced reductions in body size are greater in aquatic than terrestrial species. *Proc. Natl. Acad. Sci. U.S.A.* **109**, 19310–19314 (2012).
8. C. R. Horne, A. G. Hirst, D. Atkinson, Temperature-size responses match latitudinal-size clines in arthropods, revealing critical differences between aquatic and terrestrial species. *Ecol. Lett.* **18**, 327–335 (2015).
9. D. Pauly, *Gasping Fish and Panting Squids: Oxygen, Temperature and the Growth of Water-Breathing Animals* (International Ecology Institute, 2010).
10. W. C. E. P. Verberk *et al.*, Shrinking body sizes in response to warming: Explanations for the temperature-size rule with special emphasis on the role of oxygen. *Biol. Rev. Camb. Philos. Soc.* **96**, 247–268 (2021).
11. R. Vaquer-Sunyer, C. M. Duarte, Temperature effects on oxygen thresholds for hypoxia in marine benthic organisms: Effects of temperature in hypoxia thresholds. *Glob. Change Biol.* **17**, 1788–1797 (2011).
12. C. Deutsch, A. Ferrel, B. Seibel, H.-O. Pörtner, R. B. Huey, Climate change tightens a metabolic constraint on marine habitats. *Science* **348**, 1132–1135 (2015).
13. J. G. Rubalcaba, W. C. E. P. Verberk, A. J. Hendriks, B. Saris, H. A. Woods, Oxygen limitation may affect the temperature and size dependence of metabolism in aquatic ectotherms. *Proc. Natl. Acad. Sci. U.S.A.* **117**, 31963–31968 (2020).
14. G. E. Nilsson, S. Östlund-Nilsson, Does size matter for hypoxia tolerance in fish? *Biol. Rev. Camb. Philos. Soc.* **83**, 173–189 (2008).
15. B. A. Seibel, C. Deutsch, Oxygen supply capacity in animals evolves to meet maximum demand at the current oxygen partial pressure regardless of size or temperature. *J. Exp. Biol.* **223**, jeb210492 (2020).
16. W. W. L. Cheung *et al.*, Shrinking of fishes exacerbates impacts of global ocean changes on marine ecosystems. *Nat. Clim. Chang.* **3**, 254–258 (2012).
17. D. Pauly, W. W. L. Cheung, Sound physiological knowledge and principles in modeling shrinking of fishes under climate change. *Glob. Change Biol.* **24**, e15–e26 (2018).
18. S. Lefevre, D. J. McKenzie, G. E. Nilsson, Models projecting the fate of fish populations under climate change need to be based on valid physiological mechanisms. *Glob. Change Biol.* **23**, 3449–3459 (2017).
19. J. L. Penn, C. Deutsch, J. L. Payne, E. A. Sperling, Temperature-dependent hypoxia explains biogeography and severity of end-Permian marine mass extinction. *Science* **362**, eaat1327 (2018).
20. E. M. Howard *et al.*, Climate-driven aerobic habitat loss in the California current system. *Sci. Adv.* **6**, eaay3188 (2020).
21. C. Deutsch, J. L. Penn, B. Seibel, Metabolic trait diversity shapes marine biogeography. *Nature* **585**, 557–562 (2020).
22. K. F. Wishner *et al.*, Ocean deoxygenation and zooplankton: Very small oxygen differences matter. *Sci. Adv.* **4**, eaau5180 (2018).
23. M.-G. A. Endress *et al.*, Physiological causes and biogeographic consequences of thermal optima in the hypoxia tolerance of marine ectotherms. *bioRxiv* [Preprint] (2022). https://doi.org/10.1101/2022.02.03.478967 (Accessed 20 June 2022).
24. S. S. Killen *et al.*, Ecological influences and morphological correlates of resting and maximal metabolic rates across teleost fish species. *Am. Nat.* **187**, 592–606 (2016).
25. T. H. Boag, R. G. Stockey, L. E. Elder, P. M. Hull, E. A. Sperling, Oxygen, temperature and the deep-marine stenothermal cradle of Ediacaran evolution. *Proc. Biol. Sci.* **285**, 20181724 (2018).
26. J. H. Brown, J. F. Gillooly, A. P. Allen, V. M. Savage, G. B. West, Toward a metabolic theory of ecology. *Ecology* **85**, 1771–1789 (2012).
27. G. B. West, J. H. Brown, B. J. Enquist, A general model for the origin of allometric scaling laws in biology. *Science* **276**, 122–126 (1997).
28. J. P. DeLong, J. G. Okie, M. E. Moses, R. M. Sibly, J. H. Brown, Shifts in metabolic scaling, production, and efficiency across major evolutionary transitions of life. *Proc. Natl. Acad. Sci. U.S.A.* **107**, 12941–12945 (2010).
29. A. Clarke, N. M. Johnston, Scaling of metabolic rate with body mass and temperature in teleost fish. *J. Anim. Ecol.* **68**, 893–905 (1999).
30. J. F. Gillooly, J. P. Gomez, E. V. Mavrodiev, Y. Rong, E. S. McLamore, Body mass scaling of passive oxygen diffusion in endotherms and ectotherms. *Proc. Natl. Acad. Sci. U.S.A.* **113**, 5340–5345 (2016).
31. K. Park, W. Kim, H.-Y. Kim, Optimal lamellar arrangement in fish gills. *Proc. Natl. Acad. Sci. U.S.A.* **111**, 8067–8070 (2014).
32. Y. K. Pan, R. Ern, A. J. Esbaugh, Hypoxia tolerance decreases with body size in red drum Sciaenops ocellatus. *J. Fish Biol.* **89**, 1488–1493 (2016).
33. J. L. Penn, C. Deutsch, Avoiding ocean mass extinction from climate warming. *Science* **376**, 524–526 (2022).
34. M. L. Pinsky, R. L. Selden, Z. J. Kitchel, Climate-driven shifts in marine species ranges: Scaling from organisms to communities. *Annu. Rev. Mar. Sci.* **12**, 153–179 (2020).
35. H. K. Lotze *et al.*, Global ensemble projections reveal trophic amplification of ocean biomass declines with climate change. *Proc. Natl. Acad. Sci. U.S.A.* **116**, 12907–12912 (2019).
36. B. L. Rego, S. C. Wang, D. Altiner, J. L. Payne, Within- and among-genus components of size evolution during mass extinction, recovery, and background intervals: A case study of Late Permian through Late Triassic foraminifera. *Paleobiology* **38**, 627–643 (2012).
37. H. Song, J. Tong, Z. Q. Chen, Evolutionary dynamics of the Permian–Triassic foraminifer size: Evidence for Lilliput effect in the end-Permian mass extinction and its aftermath. *Palaeogeogr. Palaeoclimatol. Palaeoecol.* **308**, 98–110 (2011).
38. K. Kaiho, K. Takeda, M. R. Petrizzo, J. C. Zachos, Anomalous shifts in tropical Pacific planktonic and benthic foraminiferal test size during the Paleocene–Eocene thermal maximum. *Palaeogeogr. Palaeoclimatol. Palaeoecol.* **237**, 456–464 (2006).
39. T. Yamaguchi, R. D. Norris, A. Bornemann, Dwarfing of ostracodes during the Paleocene–Eocene thermal maximum at DSDP site 401 (Bay of Biscay, North Atlantic) and its implication for changes in organic carbon cycle in deep-sea benthic ecosystem. *Palaeogeogr. Palaeoclimatol. Palaeoecol.* **346–347**, 130–144 (2012).
40. D. Pauly, V. Christensen, J. Dalsgaard, R. Froese, F. Torres Jr., Fishing down marine food webs. *Science* **279**, 860–863 (1998).
41. I. A. Hatton, R. F. Heneghan, Y. M. Bar-On, E. D. Galbraith, The global ocean size spectrum from bacteria to whales. *Sci. Adv.* **7**, eabh3732 (2021).
42. T. P. Wootton, C. A. Sepulveda, N. C. Wegner, Gill morphometrics of the thresher sharks (genus Alopias): Correlation of gill dimensions with aerobic demand and environmental oxygen. *J. Morphol.* **276**, 589–600 (2015).
43. C. Deutsch, Temperature size rule metabolic index. GitHub. https://github.com/cadeutsch/Temperature_Size_Rule_Metabolic_Index. Deposited 27 February 2021.
44. R. Campbell, M. Wagner, G. Teegarden, C. Boudreau, E. Durbin, Growth and development rates of the copepod Calanus finmarchicus reared in the laboratory. *Mar. Ecol. Prog. Ser.* **221**, 161–183 (2001).
45. S. M. Leandro, P. Tiselius, H. Queiroga, Growth and development of nauplii and copepodites of the estuarine copepod Acartia tonsa from southern Europe (Ria de Aveiro, Portugal) under saturating food conditions. *Mar. Biol.* **150**, 121–129 (2006).